Available online at www.sciencedirect.com
ScienceDirect
Ceramics International 36 (2010) 1389–1395
CERAMICS INTERNATIONAL
www.elsevier.com/locate/ceramint

Microstructural and thermal properties of plasma sprayed mullite coatings

Giovanni Di Girolamo [a,*], Caterina Blasi [a], Luciano Pilloni [b], Monica Schioppa [a]

[a] ENEA, Brindisi Research Centre, 72100 Brindisi, Italy
[b] ENEA, Casaccia Research Centre, 00123 Rome, Italy

Received 1 December 2009; received in revised form 16 December 2009; accepted 25 January 2010
Available online 1 March 2010

Abstract

Thick mullite ($3Al_2O_3$–$2SiO_2$) coatings were fabricated by atmospheric plasma spraying (APS) in a mixture of crystalline and amorphous phases, as confirmed by X-ray diffraction (XRD) analysis. The coatings were isothermally heat treated in order to study recrystallization mechanism of the glassy phase. The morphology and the microstructure of both mullite feedstock and coatings were investigated by using scansion electron microscopy (SEM). The porosity of as-sprayed coating was in the range between 2 and 3% and substantially remained unchanged after thermal treatment. The thermal expansion of as-sprayed and annealed coatings was measured during heating up to the temperature of crystallization and the corresponding high-temperature extent of shrinkage was calculated. The differential scanning calorimetry (DSC) curves at different heating rates showed a sharp exothermic peak between 1243 and 1253 K, suggesting a rapid recrystallization of the amorphous phase. Finally, the heat capacity of recrystallized mullite coating was measured by DSC experiments. It was approximately 1.02×10^3 J/kg K at 373 K and increased with increasing test temperature.

Keywords: C. Thermal properties; D. Mullite; E. Thermal applications; Plasma spraying

1. Introduction

Ceramic coatings are commonly used for a wide variety of industrial applications. In particular, thermal barrier coatings (TBCs) can be engineered for thermal protection of aircraft and stationary gas turbine combustor liners, diesel engine components, heat exchanger tubes, panels of re-entry space vehicles and hot components in molten glass manufacturing plants.

To this purpose, mullite ($3Al_2O_3$–$2SiO_2$) coatings are particularly promising due to their high thermal stability, low thermal conductivity, high resistance in highly oxidative and corrosive environments, high resistance to crack propagation and high thermal shock resistance [1–6]. Previous works have demonstrated that mullite coated diesel engine components exhibited decreased surface cracking when compared to zirconia coated ones [7]. In addition, mullite coatings are suitable for environmental protection of ceramic matrix composites (CMC), *i.e.* SiC-based ceramics, against corrosion from molten salts and water vapour in combustion environments, due to their good density, chemical compatibility and thermal expansion coefficient very close to that of the substrate [8,9].

Plasma spraying is a cost-effective technique for the deposition of thick mullite coatings. The feedstock particles are melted and accelerated towards a substrate by a plasma gas stream. The molten droplets are flattened upon impact on the substrate and quenched, thus forming thin layers or splats. The inter-bonding between overlapping splats, deposited during repeated torch passes, generates a thick coating.

It has been reported that plasma spraying of mullite feedstock typically produces a structure composed of a mixture of crystalline and amorphous phases, due to the high cooling rate ($\sim 10^5$–10^6 K/s) of the molten droplets on a cold substrate [10]. During service high-temperature exposure can promote the recrystallization of the amorphous mullite. This transformation is notoriously accompanied by a volume contraction, which can generate significant thermal stresses within the coating, promoting crack growth and propagation. As a consequence, corrosive agents such as molten salts or water vapour can penetrate through the cracks and attack substrate surface, promoting a rapid degradation of the component [11,12]. It has been reported that by furnace heating SiC substrates above the crystallization temperature of mullite

* Corresponding author. Tel.: +39 0831 201503; fax: +39 0831 201581.
E-mail address: giovanni.digirolamo@enea.it (G. Di Girolamo).

0272-8842/$36.00
doi:10.1016/j.ceramint.2010.02.007

during plasma spraying a crystalline structure can be obtained [13]. However, this solution can result technologically very complex and, moreover, is not surely suitable for metal substrates, due to their high-temperature oxidation.

In the present work, thick mullite coatings were deposited by atmospheric plasma spraying. The coatings were heat treated in order to study the recrystallization mechanism and the corresponding evolution of their structural, microstructural and thermal properties. Differential scanning calorimetry experiments were performed to calculate temperature and enthalpy of crystallization. Heat capacity of recrystallized mullite coating was also measured, since it represents a significant thermal property which affects the thermal behaviour of a ceramic coating during high-temperature service. Indeed, together with thermal diffusivity and density, it influences the thermal conductivity and the rate of heat transfer from coating surface to the substrate.

2. Experimental procedure

2.1. Plasma spraying

A mullite feedstock (Sulzer Metco, Westbury, NY) with a size distribution of $-22 + 5$ μm, was processed by an atmospheric plasma spray, equipped with a F4-MB plasma torch with a 6 mm internal diameter nozzle (Sulzer Metco, Wolhen, Switzerland). The chemical composition of the feedstock used for deposition is given in Table 1.

Mullite coatings were deposited onto stainless steel substrates (25 mm × 25 mm × 4 mm) with a thickness ranging from 550 to 800 μm. Before spraying, each substrate was grit-blasted using alumina abrasive powder (Metcolite F, Sulzer Metco, Westbury, NY), to enhance the surface roughness and to guarantee the mechanical interlocking between the coating and the same substrate. Surface roughness, R_a, after blasting was about 2 μm, as measured in previous experiments.

The substrates were ultrasonically degreased in ethanol and placed on a cylindrical fixture rotating around a vertical axis in front of the plasma torch which, in turn, traversed vertically. Preliminary spray trials were previously carried out and the best set of process parameters was determined in order to produce homogeneous and thick mullite coatings. The spraying parameters used in this work are summarized in Table 2. The carrier gas flow rate, the rotation speed of powder feeder stirrer vibrator and disk were adjusted in order to ensure a powder feed rate near to 4.67×10^{-4} kg/s. The samples were not air cooled during deposition, in order to investigate the structure obtained at elevated substrate temperature. Air cooling certainly increases the quenching rate of the molten splats and, therefore, it could affect the relative amount of crystalline and amorphous phases in as-sprayed coating. To this purpose, in a previous work it has been reported that substrate cooling induces the formation of amorphous mullite in as-sprayed coating [8].

Table 1
Chemical composition of mullite feedstock (wt.%).

Al_2O_3	75.66
SiO_2	24.20
TiO_2	0.02
Fe_2O_3	0.06
CaO	0.03
MgO	0.03

Table 2
Plasma spray parameters used in this work.

Arc current (A)	500
Voltage (V)	60.8
Turntable speed (rad/s)	50
Substrate tangential speed (m/s)	1041×10^{-3}
Gun speed (m/s)	4×10^{-3}
Primary gas Ar flow rate (sm^3/s)	7.50×10^{-4}
Secondary gas H_2 flow rate (sm^3/s)	0.83×10^{-4}
Stand-off distance (mm)	100
Carrier gas flow rate (sm^3/s)	1.00×10^{-4}
Powder feed rate (kg/s)	4.67×10^{-4}
Injector diameter (mm)	2
Injector angle (°)	90
Injector distance from torch centerline axis (mm)	5
Axial injector distance from nozzle exit (mm)	6

The deposition efficiency was calculated from the feedstock mass delivered to the torch and the coating mass. The former was determined from the powder feed rate and the spraying time on the substrate.

The coatings were stripped off from their substrates by chemical etching, by using a 50/50 (vol.%) HCl–H_2O solution, which attacked the coating–substrate interface. Then, the detached ceramic coatings were cleaned by rinsing and infiltration of water, acetone and ethanol, in sequence, in order to remove acid residue and other contaminants. Free-standing coatings were isothermally annealed at 1373 K for 2 h and 1573 K for 10 h, respectively, at a heating rate of 10^{-1} K/s and then slowly furnace cooled down to room temperature, with the purpose to investigate the effect of recrystallization on their phase composition, microstructural and thermal properties.

2.2. Microstructural and thermal properties

The phase composition of both mullite feedstock and coatings was analyzed by using an X-ray powder diffractometer (XRD, PW 1880, Philips, Almelo, Netherlands), operating with a CuKα ($\lambda = 0.154186$ nm) radiation produced at 40 kV and 40 mA. The analyzed range of the diffraction angle 2θ was between 20° and 90°, by a step width of 0.02°.

Both powder morphology and coating microstructure were analyzed by a SEM-FEG (Field Emission Gun SEM Leo Gemini 1530, Carl Zeiss, Oberkochen, Germany) equipped with a high-resolution secondary electron detector (in-lens detector). Before observations, the coatings were cut with a low-speed diamond coated blade, cold mounted in vacuum in a two-part epoxy resin, ground with 20 and 10 μm diamond discs, polished with 9, 6, 3 μm diamond pastes and finished to 0.25 μm by using an alumina suspension. The pore morphology and volume were analyzed by processing SEM pictures of the cross sections by means of a free Java image analysis software (Image J, U.S. National Institutes of Health, Bethesda, Maryland). The images were acquired at different locations and at magnifications

ranging from 500× to 3000×, in order to better appreciate the fine porosity of mullite coatings. The procedure described in a previous work was herein followed [14].

The thermal expansion of as-sprayed and annealed mullite coatings (800 μm thick) was measured by using a Netzsch dilatometer (Model TMA 402, Netzsch-Gerätebau GmbH, Selb, Germany) up to 1273 K. The system here employed is mounted vertically and consists of a linear variable displacement transducer (LVDT) with thermo-stated housing. Changes in length of a sample caused by expansion or shrinkage move the quartz pushrod on the ferrite core of LVDT and cause an electrical signal in its coil. This electrical signal is amplified and recorded as a change in length. The temperature of the sample is measured and recorded by a thermocouple. Thermal expansion measurements were carried out in static air on free-standing samples, at 8.3×10^{-2} K/s rate up to crystallization temperature. To check the accuracy of the pushrod dilatometer three measurements in the same conditions were carried out on a synthetic sapphire (NS SRM 732) from room temperature to 1173 K. The calculated mean linear expansion coefficient was compared with the mean value of the standard material reported in literature (9.2×10^{-6} K^{-1}). The accuracy was equal to 3%.

Differential scanning calorimetry (DSC) analysis of mullite coatings was performed by using a Netzsch STA 429 simultaneous thermal analyzer (Netzsch-Gerätebau GmbH, Selb, Germany) equipped with a DSC-sample carrier. A sample mass of about 20 mg was heated from room temperature up to 1573 K into a closed platinum crucible in a static air atmosphere. The crystallization temperature was determined at heating rates of 5.0×10^{-2} and 16.7×10^{-2} K/s. The enthalpy of crystallization was also calculated by DSC experiments. The calorimetric sensitivity (10^{-3} V/W) was determined by employing sapphire disc as calibrant. The accuracy in ΔH measurements was about 4% with respect to the values reported for standard materials.

Moreover, the specific heat (C_p) of recrystallized mullite coating was measured from DSC curves using the ratio method, described by the following equation [15]:

$$C_{ps} = C_{pstd}\left(\frac{m_{std}}{m_s}\right)\left(\frac{\Delta T_s}{\Delta T_{std}}\right) \quad (1)$$

where the subscript *std* denotes the sapphire standard, *s* the sample, ΔT are the ordinate deflections from the sample, standard and baseline, and *m* indicates the mass. By using this method three measurements under the same test conditions were necessary. The first one was a measurement with an empty crucible, the baseline run. In the second measurement a standard material of known specific heat was employed in the same crucible. Finally, in the third run the sample being analyzed was put into the sample crucible. In this study a mullite coating sample of about 35 mg was put into a platinum crucible with lid and heated in static air, from room temperature up to 1553 K at a heating rate of 33.3×10^{-2} K/s. The three measurements, baseline, standard and sample, were performed in the same heating protocol which included (i) heating to 323 K, (ii) isothermal at 323 K for 30 min, (iii) heating to 1553 K. A synthetic sapphire disc was used as standard material (C_p of sapphire at 293 K: 0.775×10^3 J/kg K – NBS literature value). Specific heat values were calculated using the instrument software that employed the ratio method.

3. Results and discussion

3.1. Phase analysis

Fig. 1 shows the XRD pattern of mullite feedstock, as-sprayed and isothermally heat-treated coatings. The feedstock is mainly composed of orthorhombic $3Al_2O_3$–$2SiO_2$ mullite, whereas rombhohedral α-Al_2O_3 phase is present as a minor phase, according to Joint Committee on Powder Diffraction Standard (JCPDS) cards for mullite (JCPDS No. 73-1389) and α-alumina (JCPDS No. 43-1484), available at International Centre for Diffraction Data (ICDD). These crystalline phases are also present in the as-sprayed coating, as well as an amorphous glassy phase denoted by a broad hump at low 2θ angles. The formation of the amorphous phase is affected by the high quenching rate of the molten droplets, as well as by the starting size and melting rate of the sprayed particles. In turn, crystalline α-Al_2O_3 is associated to unmelted or semimolten particles. Moreover, two peaks for metastable silica-rich γ-alumina phase (JCPDS No. 10-0425) are detected in the as-sprayed coating at 46° and 67°, respectively. This last phase derived from the complete melting of sprayed particles and the high rate of heat removal from the coating surface. Free SiO_2 is not detectable in as-sprayed coating, because it is present in a glassy state. In a recent work, completely amorphous silica-rich mullite coatings were fabricated by HVOF (high velocity oxygen fuel) spraying, starting from fused and crushed feedstock characterized by an angular morphology [16].

As shown in Fig. 1, a short isothermal heat treatment of mullite coating produces the complete recrystallization of the amorphous phase, since annealed coatings are characterized by a crystalline structure mainly composed of $3Al_2O_3$–$2SiO_2$ phase (α-Al_2O_3 phase is present as a minor phase). The γ-Al_2O_3 phase recrystallizes after thermal exposure, whereas the

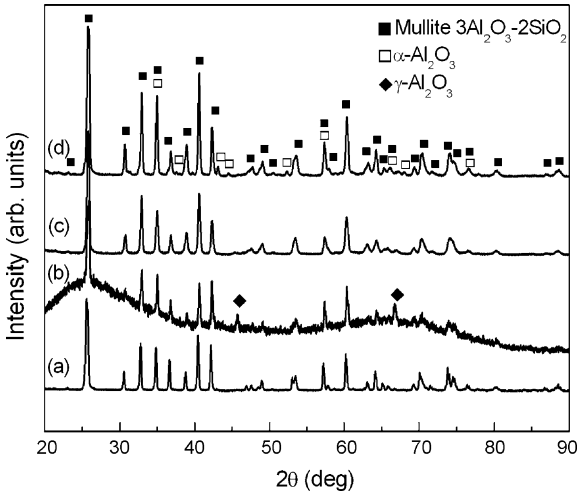

Fig. 1. XRD spectra of mullite feedstock and coatings: (a) feedstock, (b) as-sprayed coating, (c) coating treated at 1373 K, (d) coating treated at 1573 K. For sake of clarity, the peaks common to different coatings are labelled once.

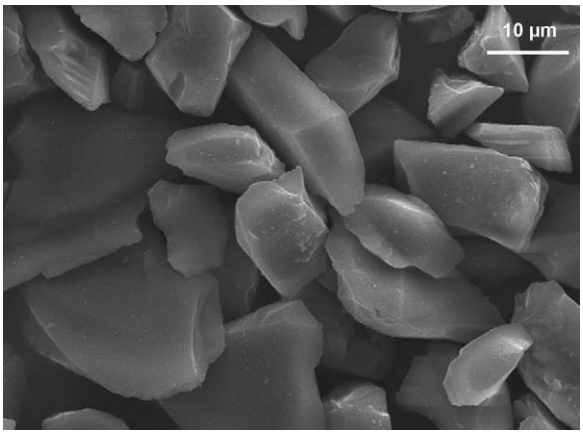

Fig. 2. Angular morphology of mullite feedstock particles.

intensity of α-Al_2O_3 peaks is lower in annealed coatings, suggesting a reaction between free alumina and silica during heat treatment. Recrystallized coatings and starting feedstock seem to show similar phase compositions, even if in heat-treated coatings the two peaks for mullite at about 26° are substituted by a new peak. Annealing temperature and time do not affect the phase composition of mullite coatings, suggesting that the recrystallization can be considered completed after 2 h of thermal exposure at 1373 K.

3.2. Microstructure

Fig. 2 shows the morphology of fused and crushed mullite particles, characterized by an irregular blocky and angular shape. The deposition rate, measured by a digital micrometer with a resolution of 1 μm, was equal to 8.20 ± 0.69 μm per torch pass. The deposition efficiency is defined as the ratio of the coating weight to the weight of the total feedstock. The measured real deposition efficiency was found to be $23.90 \pm 2.04\%$. The low deposition efficiency is strongly associated to the morphology of the feedstock. Indeed, part of the starting particles was not carried by plasma gas stream, remained unmelted and was not deposited on the substrate.

The picture shown in Fig. 3 illustrates the microstructural features of as-sprayed mullite coating, whereas Fig. 4 shows the

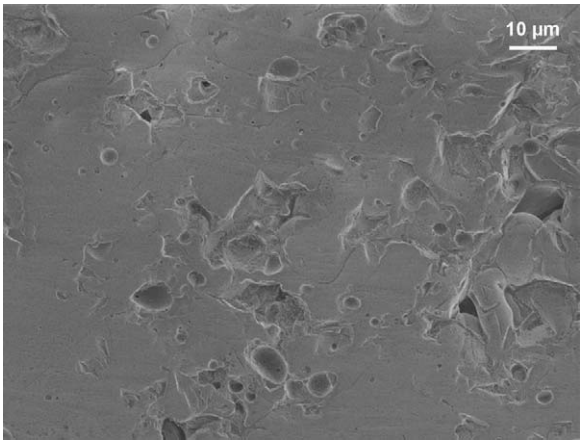

Fig. 3. Cross-sectional microstructure of as-sprayed mullite coating.

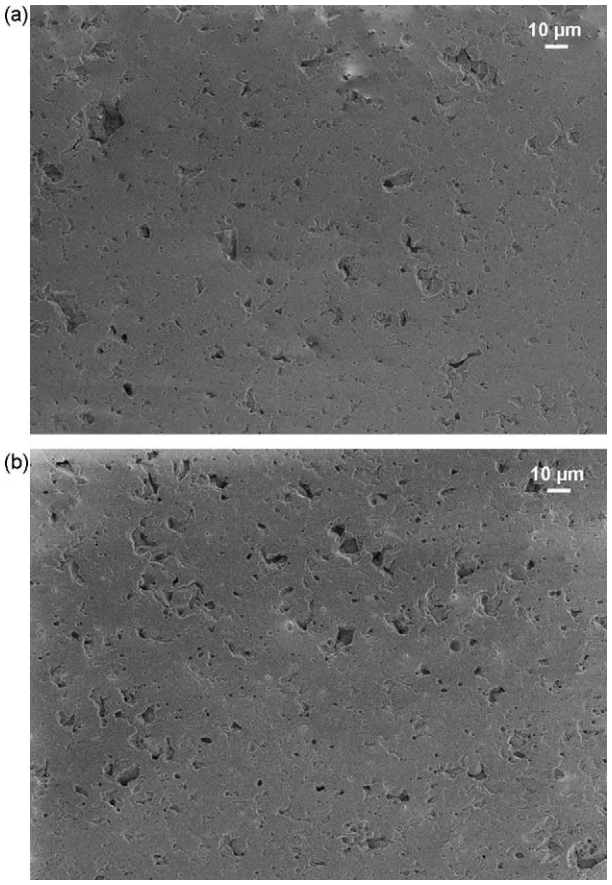

Fig. 4. Cross-sectional microstructure of annealed mullite coatings: (a) coating treated at 1373 K and (b) coating treated at 1573 K.

cross-section of heat-treated coatings. The as-sprayed coating shows good homogeneity and integrity, as well as a reduced porosity, due to the narrow size distribution, good melting degree and high kinetic energy of feedstock particles. It does not exhibit a lamellar structure, as found for other plasma sprayed ceramic coatings. The porosity, measured by Image Analysis, was found to be $2.44 \pm 0.45\%$ and substantially remained unchanged after thermal treatment. Indeed, the slight increase in porosity mean value lies in the error range (the porosity of heat-treated coatings is lower than 3%). It has recently been reported by Berghaus et al. that the porosity of mullite coatings sprayed by HVOF Spraying, by employing a spray distance similar to that used in this work, was in the range between 3 and 4% [17]. So, the values here reported are comparable to those. Instead, Rohan et al. have reported higher values for their mullite coatings, manufactured using a high-throughput water-stabilized plasma spray system [5].

It should be noted that a dense coating is particularly promising to be used as an intermediate layer in thermal or environmental barrier coating systems. Indeed, a lower gas permeability is expected, thus reducing high-temperature oxidation of the substrate. Taking into consideration an EBC system, it should be noted that an upper ceramic top coat should be applied on plasma sprayed mullite layer in order to avoid the volatilization of silica via reaction with water vapour at temperatures higher than 1473 K [12].

According to image analysis, the microstructure of mullite coatings mainly includes circular or elliptical fine pores ($d < 3$ μm), which derived from gas entrapped under the liquid droplets and are homogeneously distributed. More large pores ($d > 3$ μm) are associated with filling defects in the coating structure, caused by unmelted or partially melted particles, and are not homogeneously distributed. To this purpose, the contribution of pull-out effects during polishing has to be taken in account.

Taking into consideration the thermal effects of thermal spraying, it should be noted that significant cracks may be produced from mullite crystallization during cooling to room temperature. Indeed, part of the previously deposited material can recrystallize during the next paths of the plasma torch. In a previous work, this effect has been considered as the main reason for the formation of tensile stresses which lead to the growth of segmented cracks, whose width was in the range between 2 and 30 μm, depending to a large extent on the spray distance [18]. However, in the present experiment no through-thickness cracks have been detected in as-sprayed coating. To this purpose, higher values for spray distance and plasma gas mass flow rate have been chosen. The increase of the spray distance typically reduces both velocity and temperature of sprayed particles, while the increase of the mass flow rate increases the velocity and slightly decreases coating surface temperature.

As previously reported, isothermal post-heat treatment of as-sprayed mullite coatings produces the recrystallization of the glassy phase. This transformation is notoriously accompanied by a volume contraction and promotes further stresses, leading to the formation of crack networks in the coating. However, heat-treated coatings are free of macrocracks, suggesting the development of contained thermal stresses. Instead, some microcracks are observable at higher magnification, but only in isolated regions within the coating. Fig. 5 shows these microstructural defects in a mullite coating treated at 1573 K for 10 h. It should be noted that the high crystallinity of heat-treated mullite coatings may depend on the presence of microstructural defects, which represent preferential sites for nucleation.

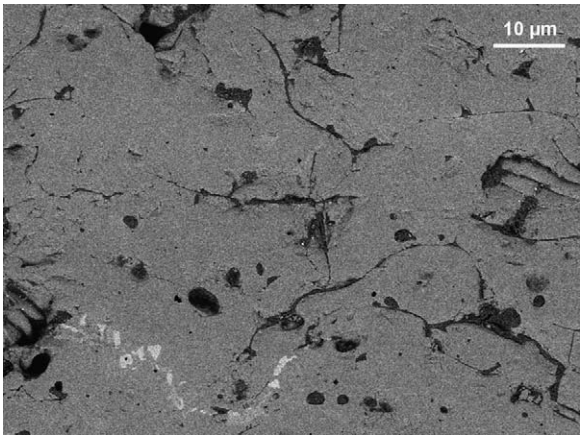

Fig. 5. A high-porosity region in a mullite coating treated at 1573 K (cross-section). Some microcracks are detectable in the microstructure.

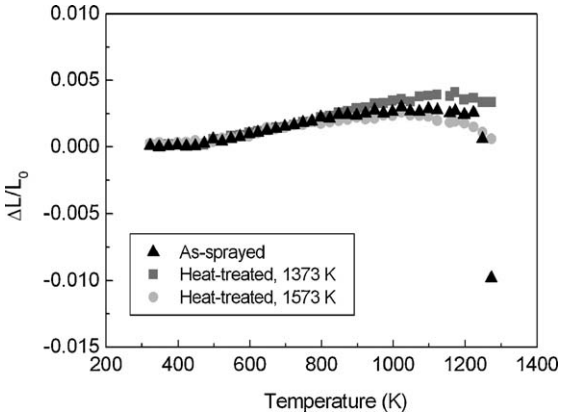

Fig. 6. Thermal expansion of as-sprayed and annealed mullite coatings. In as-sprayed coating a volume contraction is observable below 1273 K.

Obviously, since free-standing coatings were tested, the recrystallization effect was only considered, whereas the influence of the thermal expansion mismatch between coating and substrate during high-temperature exposure was not investigated.

3.3. Thermal properties of amorphous and recrystallized coatings

The thermal expansion of as-sprayed and annealed mullite coatings is shown in Fig. 6. The low thermal expansion below 473 K is associated to the low thermal energy which is not high enough as to provide expansion [19]. At higher temperature the thermal expansion is approximately linear. The as-sprayed coating shows a volume contraction below 1273 K, associated to the crystallization of the amorphous mullite. The measured shrinkage is of about 1%. The thermal expansion coefficients of mullite coatings have been measured between 473 and 1173 K and are summarized in Table 3. It can be seen that the thermal expansion coefficient changes with increasing both annealing temperature and time.

Fig. 7 shows the DSC curve obtained for as-sprayed mullite coating at a heating rate of 5.0×10^{-2} K/s. The DSC curve exhibits a sharp and strong exothermic peak around 1244 K, attributed to the rapid recrystallization of the amorphous mullite during heating [8,20]. As reported in the previous sections, during plasma spray processing mullite feedstock excurses a very high temperature regime and isolated regions of molten SiO_2-rich aluminosilicates are formed and then quenched into the glassy phase. This last one has a temperature window for exothermic crystallization, which rapidly takes place during the relatively short DTA experiment. This phase transformation, known as Hedvall effect, is associated to exothermicity. Indeed,

Table 3
Thermal expansion coefficients for as-sprayed and annealed mullite coatings.

Sample	Temperature range (K)	α (K^{-1})
As-sprayed	473–1173	3.8×10^{-6}
Heat-treated, 1373 K	473–1173	5.6×10^{-6}
Heat-treated, 1573 K	473–1173	2.7×10^{-6}

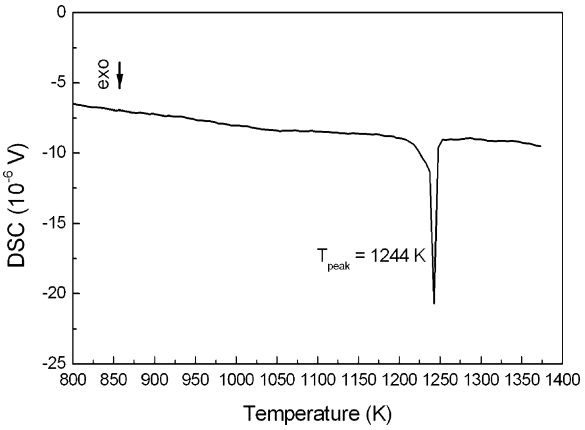

Fig. 7. DSC curve of as-sprayed mullite coating at a heating rate of 5×10^{-2} K/s. The exothermic peak denotes the rapid crystallization of the glassy phase.

the reaction between free alumina and glassy silica produces the formation of a new mullite phase with orthorhombic structure, whose composition may not be identical to that of the starting feedstock. It is interesting to point out that the crystallization effect could be bypassed during thermal shock experiments on plasma sprayed mullite coatings [4].

As illustrated in Fig. 8, the top temperature of the exotherm peak increases with increasing heating rate, as described by Takei et al. [21]. The crystallization temperature is found to be 1253 K for a heating rate of 16.7×10^{-2} K/s. Schneider et al. suggested that the driving force of 1253 K reaction process is the dissappearence of (Al O)-pentahedra due to its sudden instability in this temperature range and subsequent crystallization either of mullite or γ-Al_2O_3 [22].

As shown in Fig. 9, the enthalpy of crystallization, determined from DSC measurements at 5×10^{-2} K/s heating rate, was of -295×10^3 J/kg between 1217 and 1250 K. To this purpose, Douy et al. have studied the variation of the enthalpy with the global composition of the sample (Al_2O_3–SiO_2 systems). With increasing the alumina content, the enthalpy increased regularly in the domain of mullite crystallization and decreased in the domain of spinel crystallization. The maximum value was found in 60–70 mol% Al_2O_3 composition range, when a maximum

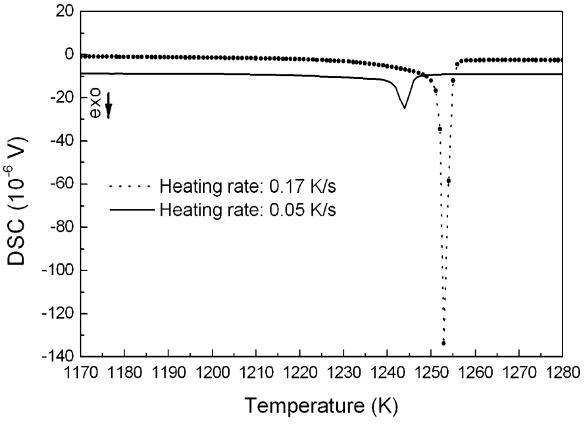

Fig. 8. DSC curves of as-sprayed mullite coating, measured at different heating rates.

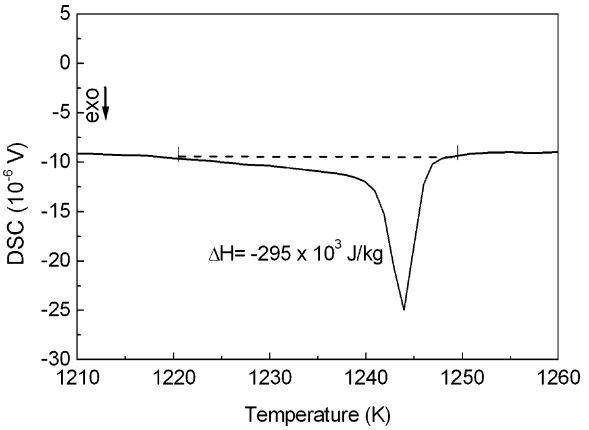

Fig. 9. Integral of DSC crystallization peak for enthalpy calculation.

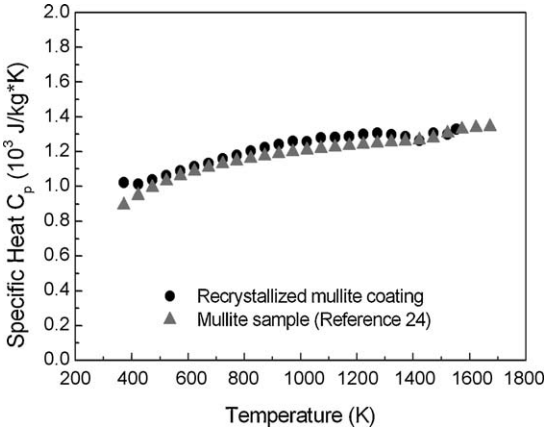

Fig. 10. C_p curve of recrystallized mullite coating derived from averaging and smoothing data. The experimental data are compared to earlier published ones.

amount of mullite crystallized. The corresponding enthalpy was of about -290×10^3 J/kg for 60 mol% Al_2O_3 [23].

Fig. 10 shows the specific heat capacity of a mullite coating treated at 1373 K for 2 h in the range between 373 and 1553 K. Starting from a value of 1.02×10^3 J/kg K at 373 K, the specific heat increases over the entire temperature range. The experimental C_p curve of recrystallized mullite coating is very close to that obtained by Hildmann et al. on their single-crystal mullite samples up to 1553 K [24]. As described in this previous work, the C_p curve shows the typical temperature-dependent shape up to 1373 K, whereas at higher temperatures the C_p curve shows an anomalous trend, characterized by a significant increase of heat capacity. This behaviour has been observed in both single-crystal and polycrystalline mullite samples and it is similar to typical glass transition. According to the authors, it does not correspond to any phase transition, but it is probably determined by dynamic site-exchange processes between tetrahedral cations and oxygen vacancies in mullite structure at high temperature.

4. Conclusions

Thick plasma sprayed mullite coatings were deposited by atmospheric plasma spraying in a mixture of crystalline and

amorphous phases. The effects of recrystallization induced by heat treatment on as-produced coatings were investigated.

Heat-treated coatings showed a crystalline structure, mainly composed of mullite ($3Al_2O_3$–$2SiO_2$), due to the recrystallization of the glassy phase and γ-Al_2O_3. Both as-sprayed and annealed mullite coatings showed a reduced porosity (between 2 and 3%), mainly composed of fine and homogeneously distributed pores. No significant microcracks were observed in the coatings after thermal annealing up to 1573 K.

The recrystallization of the glassy phase was clearly observable during the measurements of the thermal properties on as-sprayed coatings. Thermal expansion curve showed a contraction at about 1253 K and, at the same time, DSC curve showed a sharp and strong exothermic peak, associated to the rapid recrystallization of the amorphous mullite during heating. The temperature of crystallization increased with increasing heating rate. The enthalpy of crystallization at 5.0×10^{-2} K/s heating rate was equal to -295×10^3 J/kg. Finally, the specific heat capacity of recrystallized mullite coating was approximately 1.02×10^3 J/kg K at 373 K and increased over the entire temperature range.

In conclusion, partially amorphous mullite coatings are surely promising for thermal protection of metal components in diesel engines and glass-melting furnaces, since the maximum temperatures expected during service are lower than the recrystallization temperature of the amorphous phase. In addition, we found that the effects of recrystallization on coating microstructure are rather contained for free-standing specimens composed of a mixture of crystalline and amorphous phase.

Follow-up works will investigate the application of mullite coatings for environmental protection of SiC-based substrates.

References

[1] S. Varadarajan, A.K. Pattanaik, V.K. Sarin, Mullite interfacial coatings for SiC fibers, Surf. Coat. Technol. 139 (2001) 153–160.

[2] X.Q. Cao, R. Vassen, D. Stoever, Ceramic materials for thermal barrier coatings, J. Eur. Ceram. Soc. 24 (2004) 1–10.

[3] C. Bartuli, L. Lusvarghi, T. Manfredini, T. Valente, Thermal spraying to coat traditional ceramic substrates: case studies, J. Eur. Ceram. Soc. 27 (2007) 1615–1622.

[4] P. Ramaswamy, S. Seetharamu, K.B.R. Varma, K.J. Rao, Thermal shock characteristics of plasma sprayed mullite coatings, J. Thermal Spray Technol. 7 (4) (1998) 497–504.

[5] P. Rohan, K. Neufuss, J. Matejicek, J. Dubsky, L. Prchlik, C. Holzgartner, Thermal and mechanical properties of cordierite, mullite and steatite produced by plasma spraying, Ceram. Int. 30 (2004) 597–603.

[6] H. Schneider, J. Schreurer, B. Hildmann, Structure and properties of mullite—a review, J. Eur. Ceram. Soc. 28 (2008) 329–344.

[7] K. Kokini, Y.R. Takeuchi, B.D. Choules, Surface thermal cracking of thermal barrier coatings owing to stress relaxation: zirconia vs. mullite, Surf. Coat. Technol. 82 (1996) 77–82.

[8] K.N. Lee, R.A. Miller, N.S. Jacobson, New generation of plasma sprayed mullite coatings on silicon carbide, J. Am. Ceram. Soc. 78 (3) (1995) 705–710.

[9] K.N. Lee, D.S. Fox, J.I. Eldridge, D. Zhu, R.C. Robinson, N.P. Bansal, R.A. Miller, Upper temperature limit of environmental barrier coatings based on mullite and BSAS, J. Am. Ceram. Soc. 86 (8) (2003) 1299–1306.

[10] J.G. Fisher, K. Chang, P.F. James, P.F. Messer, H.A. Davies, Ceramic flake formation in the aluminosilicate system by plasma spraying, J. Mater. Sci. 40 (2005) 1625–1632.

[11] K.N. Lee, Current status of environmental barrier coatings for Si-based ceramics, Surf. Coat. Technol. 133/134 (2000) 1–7.

[12] K.N. Lee, Key durability issues with mullite-based environmental barrier coatings for Si-based ceramics, Trans. ASME 122 (2000) 632–636.

[13] K.N. Lee, R.A. Miller, Oxidation behavior of mullite-coated SiC and SiC/SiC composites under thermal cycling between room temperature and 1200 °C–1400 °C, J. Am. Ceram. Soc. 79 (3) (1996) 620–626.

[14] M. Alfano, G. Di Girolamo, L. Pagnotta, D. Sun, Processing, microstructure and mechanical properties of air plasma sprayed ceria–yttria co-stabilized zirconia coatings, Strain (2010), doi:10-1111/j.1475-1305.2009.00659.x.

[15] B. Henderson, W.D. Emmerich, E. Wassmer, Measurement of Specific Heat and Energetics of Curing and Decomposition of a Glass-filled Polymer Composites, Netzsch Gerätebau GmbH, Selb, Germany (1988).

[16] J. Leivo, T.E. Varis, E. Turunen, M. Vippola, K. Rissa, U. Kanerva, J. Silvonen, T.A. Mantyla, Influence of the elementary mixing scale on HVOF-sprayed coatings derived from nanostructured aluminosilicate/mullite feedstock, Surf. Coat. Technol. 203 (2008) 335–344.

[17] J.O. Berghaus, B.R. Marple, High-velocity oxy-fuel (HVOF) suspension spraying of mullite coatings, J. Thermal Spray Technol. 17 (5/6) (2008) 671–678.

[18] S. Latzel, R. Vassen, D. Stover, New environmental barrier coating system on carbon-fiber reinforced silicon carbide composites, J. Thermal Spray Technol. 14 (2) (2005) 268–272.

[19] G. Brunauer, F. Frey, H. Boysen, H. Schneider, High temperature thermal expansion of mullite: an in situ neutron diffraction study up to 1600 °C, J. Eur. Ceram. Soc. 21 (2001) 2563–2567.

[20] M. Schmücker, H. Schneider, M. Poorteman, F. Cambier, R. Meinhold, Constitution of mullite glasses produced by ultra-rapid quenching of plasma-sprayed melts, J. Eur. Ceram. Soc. 15 (1995) 1201–1205.

[21] T. Takei, Y. Kameshima, A. Yasumori, K. Okada, Crystallization kinetics of mullite from Al_2O_3–SiO_2 glasses under non-isothermal conditions, J. Eur. Ceram. Soc. 21 (2001) 2487–2493.

[22] H. Schneider, D. Voll, B. Saruhan, J. Sanz, G. Schrader, C. Rüscher, A. Mosset, Synthesis and structural characterization of non-crystalline mullite precursors, J. Non-Cryst. Solids 178 (1994) 262–271.

[23] A. Douy, Crystallisation of amorphous spray-dried precursors in the Al_2O_3–SiO_2 system, J. Eur. Ceram. Soc. 26 (2006) 1447–1454.

[24] B. Hildmann, H. Schneider, Heat capacity of mullite: new data and evidence for a high-temperature phase transformation, J. Am. Ceram. Soc. 87 (2) (2004) 227–234.